Fully relativistic *B*-spline *R*-matrix calculations for electron collisions with mercury

O. Zatsarinny* and K. Bartschat†
Department of Physics and Astronomy, Drake University, Des Moines, Iowa 50311, USA
(Received 21 February 2009; published 28 April 2009)

Results from a fully relativistic 36-state Dirac *B*-spline *R*-matrix (close-coupling) calculation for *e*-Hg collisions are reported. Angle-integrated and angle-differential cross sections for elastic scattering and excitation of the $(6s6p)\ ^3P^o_{0,1,2}$ and $(6s6p)\ ^1P^o_1$ states are compared to experimental data and predictions from other theories. We generally obtain a significant improvement in the agreement between experiment and theory compared to previous distorted-wave and close-coupling attempts, in particular, for the near-threshold region that is dominated by various $6s6p^2$ negative-ion resonances.

DOI: 10.1103/PhysRevA.79.042713 PACS number(s): 34.80.Dp

I. INTRODUCTION

For many years, electron collisions with mercury atoms have provided a rich field for experimental and theoretical studies. As a heavy target with nuclear charge $Z=80$, though still looking in many aspects such as helium, numerous theoretical attempts have been made to describe this collision system. Without aiming for a comprehensive list of references, these methods include fully relativistic potential scattering for elastic collisions by Walker [1], McEachran and Stauffer [2], Sienkiewicz [3,4], Haberland and Fritsche [5], and McEachran and Elford [6], semi-relativistic and fully relativistic distorted-wave calculations for excitation by Bartschat and Madison [7] and Srivastava *et al.* [8], and semirelativistic as well as fully relativistic *R*-matrix (close-coupling) calculations by Scott *et al.* [9], Bartschat [10], and Wijesundera *et al.* [11], to name just a few.

On the experimental side, angle-integrated, momentum-transfer, and angle-differential cross sections were reported, for example, by Jost and Ohnemus [12], England and Elford [13], Holtkamp *et al.* [14], Peitzmann and Kessler [15], Panajotovic *et al.* [16], and Zubek *et al.* [17,18] for both elastic and inelastic *e*-Hg collisions. In addition to cross sections, there is a vast database of measurements and calculations available for the spin-polarization function [19], various spin asymmetries, and spin-dependent electron-impact coherence parameters. Much of the recent work in this area, which is beyond the scope of the present paper, was reviewed by Andersen *et al.* [20] and summarized by Andersen and Bartschat [21].

In addition to providing an excellent test ground for assessing the reliability of various theoretical approaches to the problem, electron collisions with mercury are of significant interest in the modeling of fluorescent and high-intensity discharge lamps [22,23]. The data sets suggested by Rockwood [24] are widely used for plasmas containing mercury, in spite of the doubts raised about their appropriateness [10,16,18].

Over the past two decades, significant progress has been made in the theoretical description of electron collisions with light quasi-one- and quasi-two-electron targets such as H, He, the alkali metals, and the alkaline-earth metal elements. In addition to advanced first-order and even second-order distorted-wave [25] methods, the convergent close-coupling (CCC) [26] and the *R*-matrix with pseudostates (RMPS) [27] approaches have been highly successful. Only recently, however, the CCC and the RMPS methods were extended to fully relativistic versions [28,29], with test applications once again to relatively simple targets.

For more complex targets, such as the heavy noble gases, the increasing importance of relativistic effects and correlations between various subshells requires an approach that can handle the strong term dependence of the one-electron orbitals in an efficient manner. Over the past decade, we have developed a highly flexible *B*-spline *R*-matrix (BSR) method, starting with a nonrelativistic framework [30] before moving on to a semirelativistic Breit-Pauli version [31] and, most recently, a fully relativistic scheme based on the Dirac-Coulomb Hamiltonian [32]. The two key ideas of the method are the use of term-dependent and hence nonorthogonal sets of one-electron orbitals in the target description and the employment of *B*-splines as the underlying effectively complete basis to expand the wave function of the projectile. In the meantime, the Breit-Pauli version of the BSR complex has been published [33] and the Dirac-based *B*-spline *R*-matrix (DBSR) approach was applied to *e*-Au collisions [34,35].

In the latter calculation, we successfully allowed for the opening of the $5d$ subshell in order to describe the core-valence correlations in an *ab initio* manner. The next level of complexity occurs in moving from Au to Hg, i.e., treating two rather than one electron in the valence shells. This work is the subject of the present paper, which is organized as follows. The numerical approach is described in Sec. II, separated into the target structure and the collision parts. Our results for angle-integrated and angle-differential cross sections are presented in Sec. III and compared to a variety of experimental benchmark data and predictions from other theories. Finally we summarize our conclusions in Sec. IV and also provide an outlook regarding the future of electron collisions with heavy complex targets.

II. COMPUTATIONAL MODEL

The calculations reported in this paper were performed using the *R*-matrix (close-coupling) approach. Specifically,

*oleg.zatsarinny@drake.edu
†klaus.bartschat@drake.edu

we employed our newly developed Dirac *B*-spline *R*-matrix approach. This program is an extension of the BSR complex [33] to the fully relativistic Dirac scheme. It was described in detail in recent applications to *e*-Cs [32] and *e*-Au [34,35] collisions. As mentioned already in Sec. I, the distinguishing features of the method are (i) the ability to use term-dependent, and hence nonorthogonal, sets of one-electron Dirac spinors in the target description and (ii) *B*-splines as the underlying, effectively complete basis to expand the wave function of the projectile. Furthermore, it is an *all-electron approach* and hence core-valence correlation effects (such as the core polarization) can be described *ab initio*.

In the present calculations, we used the Dirac-Coulomb Hamiltonian to describe both the *N*-electron target and the $(N+1)$-electron collision system. The total wave function for each partial-wave symmetry was constructed from four-component Dirac spinors. Note that the radial functions for the large and small components were expanded in separate *B*-spline bases of different order. This allowed us to avoid the occurrence of unphysical pseudostates [36]. We used a semiexponential grid for the *B*-spline knot sequence and a relatively large number (111) of splines to cover the inner region up to the *R*-matrix radius of $50a_0$, where $a_0=0.529\times10^{-10}$ m denotes the Bohr radius. This large number of splines was required to correctly describe the finite-size nuclear model with a Fermi potential adopted in the present work.

We begin by describing the structure model used for the Hg target in Sec. II A. This is followed by a summary of the collision calculation. Unless specified otherwise, atomic units are used throughout this paper.

A. Structure calculation

The structure calculation of the Hg target states is complicated by the fact that we need both the two-electron $5d^{10}6snl$ valence states and the core-excited $5d^96s^2nl$ states. Some of the core-excited states lie among the valence states and strongly affect the resonance structure at low scattering energies. Another complication arises from the fact that both valence and core-valence correlations are important for the ground state and the low-lying excited states of Hg. In all previous works on *e*-Hg collisions that we are aware of, the core-valence correlation was either neglected entirely or approximated by a semiempirical core-polarization potential. Although such a potential simplifies the calculations significantly and can provide accurate excitation energies and oscillator strengths, the question always remains how well the model potential can simulate *all* core-valence correlation, including nondipole contributions. In the present approach, we therefore included the core-valence correlation *ab initio* by adding target configurations with an excited core. However, direct multiconfiguration calculations in this case usually lead to very large expansions, which can hardly be used in subsequent scattering calculations. For this reason, we used the *B*-spline box-based close-coupling method [37] to generate the target states. This method also provides a way to accurately describe the strong interaction between the valence and core-excited states.

Specifically, the calculation of the target states included the following steps. We started by generating the core orbitals from a Hg^{2+} Dirac-Fock calculation using the GRASP2K relativistic atomic-structure package [38]. Next, the valence $6s$, $6p$, $6d$, and $7s$ orbitals were generated in a frozen-core calculation for Hg^+. We then obtained the core-excited $5d^96s^2$ states of Hg^+ in separate multiconfiguration Dirac-Fock (MCDF) calculations with fully relaxed $5d$ and $6s$ orbitals, also accounting for configuration interaction with the $5d^96p^2$ states. Finally, we obtained the $5d^96s6p$ core-excited states of Hg^+ in the term-averaged approximation, but again with relaxed $6s$ and $6p$ orbitals.

All these states of Hg^+ were then used as target states in *B*-spline bound-state close-coupling calculations to generate the low-lying states of atomic Hg. The corresponding close-coupling expansion had the structure

$$\begin{aligned}\Phi(5d^{10}6snl,J\pi) = {}& \mathcal{A}\sum_i \{\varphi(5d^{10}6s)\phi(n_il_i)\}^{J\pi} \\ & + \mathcal{A}\sum_i \{\varphi(5d^9[6s^2+6p^2])\phi(n_il_i)\}^{J\pi} \\ & + \mathcal{A}\sum_i \{\varphi(5d^{10}6p)\phi(n_il_i)\}^{J\pi} \\ & + \mathcal{A}\sum_i \{\varphi(5d^{10}7s)\phi(n_il_i)\}^{J\pi} \\ & + \mathcal{A}\sum_i \{\varphi(5d^{10}6d)\phi(n_il_i)\}^{J\pi} \\ & + \mathcal{A}\sum_i \{\varphi(5d^96s6p)\phi(n_il_i)\}^{J\pi} \\ & + a\varphi(5d^{10}6s^2) + b\varphi(5d^{10}6p^2), \end{aligned} \tag{1}$$

where $\mathcal{A}$ denotes the antisymmetrization operator. The unknown large and small radial components for the outer valence electron, $\phi(n\ell)$, were expanded in individual *B*-spline bases. The coefficients of these expansions were found by diagonalizing the Dirac-Coulomb Hamiltonian with the additional requirement that the wave functions vanish at the boundary. More details of this procedure can be found in [32].

The first two sums in Eq. (1) represent the physical valence and core-excited states under consideration. The next three sums were included to describe the valence correlations, while the last sum accounts for the core-valence correlation. Although the above close-coupling expansion can also generate the $5d^{10}6s^2$ and $5d^{10}6p^2$ states, we explicitly added the initial one-configuration wave functions of these states for a more extended description of the term dependence in the $6s$ and $6p$ orbitals for this case.

The above scheme yields nonorthogonal term-dependent orbitals $\phi(n\ell)$ for each Hg state. The present approach differs from our previous calculations for Cs and Au, where the core-valence correlation was described with additional, specially designed correlated orbitals. Accounting for the various terms and the coupling between them, the expansion (1) contained 28 core states. This scheme led to relatively small (40–80 terms) configuration-interaction expansions for the final target states of Hg. On the other hand, it yielded a large

TABLE I. Target states of Hg used in the DBSR model. Most of the experimental energies are taken from the NIST database [39] except for energies marked with an asterisk. The latter were given by Lear and Morris [40].

Configuration	Term	Expt. (eV)	Theory (eV)	Diff. (eV)
$6s^2$	$^1S_0$	0.000	0.000	0.000
$6s6p$	$^3P_0^o$	4.667	4.590	−0.078
$6s6p$	$^3P_1^o$	4.887	4.821	−0.065
$6s6p$	$^3P_2^o$	5.461	5.401	−0.060
$6s6p$	$^1P_1^o$	6.704	6.848	0.144
$6s7s$	$^3S_1$	7.730	7.794	0.064
$6s7s$	$^1S_0$	7.926	7.953	0.027
$5d^96s^26p$	$^3P_2^o$	8.541	8.533	−0.007
$6s7p$	$^3P_0^o$	8.619	8.613	−0.006
$6s7p$	$^3P_1^o$	8.637	8.630	−0.007
$5d^96s^26p$	$^3D_3^o$	8.794*	8.816	0.021
$6s7p$	$^3P_2^o$	8.829	8.842	0.014
$6s7p$	$^1P_1^o$	8.839	8.845	0.006
$6s6d$	$^3D_1$	8.845	8.847	0.002
$6s6d$	$^1D_2$	8.844	8.850	0.006
$6s6d$	$^3D_2$	8.852	8.866	0.014
$6s6d$	$^3D_3$	8.856	8.868	0.011
$6s8s$	$^3S_1$	9.170	9.169	−0.001
$6s8s$	$^1S_0$	9.225	9.215	−0.010
$5d^96s^26p$	$^3F_4^o$	9.540	9.513	−0.027
$5d^96s^26p$	$^1D_2^o$	9.755	9.730	−0.025
$5d^96s^26p$	$^1P_1^o$	9.772	9.745	−0.027
$5d^96s^26p$	$^1F_3^o$	9.934*	9.877	−0.057
$5d^96s^26p$	$^3F_3^o$		9.908	
Ionization limit		10.438		
$5d^96s^26p$	$^3F_2^o$		10.602	
$5d^96s^26p$	$^3P_1^o$	11.005	11.104	0.099
$5d^96s^26p$	$^3P_0^o$		11.111	
$6p^2$	$^3P_0$	11.170	11.224	0.054
$5d^96s^26p$	$^3D_1^o$	11.622	11.583	−0.039
$5d^96s^26p$	$^3D_2^o$		11.703	
$6p^2$	$^3P_1$	11.652	11.787	0.135
$6p^2$	$^3P_2$	11.926*	11.897	−0.029
$5d^96s^27s$	$^3D_3^o$	12.039*	11.939	−0.100
$5d^96s^27s$	$^3D_2^o$	12.065*	11.963	−0.102
$6p^2$	$^1D_2$		12.253	
$6p^2$	$^1S_0$		14.248	

amount of different nonorthogonal orbitals (about 900), which were used for the description of all target states.

The number of physical states that we can generate in this method depends on the size a of the R-matrix box. Choosing $a=50a_0$ allowed us to obtain a good description for all low-lying states of Hg up to $(6s8s)\ ^1S_0$. The target states included in the present scattering calculations are listed in Table I. We see that the present method allows us to reproduce all excitation energies with an accuracy of better that 0.15 eV, including the core-excited states. We consider this an excellent start, given the complete *ab initio* character of these calculations. In the subsequent scattering calculations, however, we used the experimental excitation energies. This allowed us to compare directly to experiment, especially regarding the near-threshold resonance structure. It is worth noting that our procedure of adjusting the target energies effectively corresponds to small stretches or contractions of the energy scale between the various thresholds [33]. Since we do not force orthogonality between the target and the projectile orbitals (see Sec. II B), we do not have to include $(N+1)$-electron "bound-bound" terms in the close-coupling expansion of the collision problem. As a result, using the experimental thresholds does not carry the danger of otherwise possible inconsistencies in the relative positions of the N-electron target and the $(N+1)$-electron resonance states.

TABLE II. Contributions to the static dipole polarizability of the Hg ground state in the DBSR model. Here kp,kf and np,nf stand for contributions from the ionization continuum and the remaining states in the Rydberg series. The oscillator strengths are given as the unweighted average of several sets of experimental values. See Migdalek [42] for references and more details.

Upper level	Oscillator strength	Polarizability (a_0^3)	Experiment
$(5d^{10}6s6p)\ ^1P_1^o$	1.147	18.474	1.16
$(5d^{10}6s6p)\ ^3P_1^o$	0.018	0.435	0.024
$(5d^{10}6s7p)\ ^1P_1^o$	0.022	0.208	
$(5d^{10}6s8p)\ ^1P_1^o$	0.019	0.154	
$(5d^96s^26p)\ ^1P_1^o$	0.203	1.583	
$(5d^96s^26p)\ ^3P_1^o$	0.495	2.976	
$(5d^96s^26p)\ ^3D_1^o$	0.182	0.994	
$(5d^96s^27p)\ ^1P_1^o$	0.086	0.386	
$(5d^96s^28p)\ ^1P_1^o$	0.027	0.110	
$(5d^96s^27p)\ ^3P_1^o$	0.044	0.154	
$6skp$		3.426	
$5d^96s^2(np+kp)$		2.143	
$5d^96s^2(nf+kf)$		2.993	
Total		34.036	33.9[a]

[a]Reference [41].

The oscillator strengths for transitions from the ground state and the corresponding contributions to the polarizability are given in Table II. The oscillator strength for the $(6s^2)\ ^1S_0 \rightarrow (6s6p)\ ^1P_1^o$ resonance transition obtained using the above method is close to the average value of the available experimental results. This transition provides the principal contribution to the polarizability of the ground state. Nevertheless, core excitations to the $5d^96s^2np$ and $5d^96s^2nf$ states are also very important, along with excitation to the $5d^{10}6snp$ Rydberg and $5d^{10}6skp$ continuum states. Our theoretical value of $34.036a_0^3$ for the static dipole polarizability, obtained by including all states that can be generated from expansion (1), is very close to the experimental result of $33.9a_0^3$ [41], thereby providing additional support for the accuracy and completeness of our B-spline expansion for the bound states of Hg. In the subsequent collision calculation

(see Sec. II B), we were able to include the 36 target states listed in Table I. These states account for about 72% ($24.7a_0^3$) of the total polarizability. The omission of the other states may affect particularly the results for the elastic cross section at low energies, but the above model is as much as we could handle with our current computer codes and the available computational resources.

B. Collision calculation

The present DBSR close-coupling expansion contained 36 target states with the following configurations: $(5d^{10}6s^2)$, $(5d^{10}6s6p)$, $(5d^{10}6s7s)$, $(5d^{10}6s7p)$, $(5d^{10}6s6d)$, $(5d^{10}6s8s)$, $(5d^{10}6p^2)$, $(5d^96s^26p)$, and $(5d^96s^27s)$. Note once again the occurrence of states with single-electron excitation out of the $5d^{10}$ subshell. As mentioned above, the size of the chosen close-coupling expansion was restricted by the available computational resources. Note in particular that the $(5d^96s^26d)$ and $(5d^96s^24f)$ core-excited states had to be omitted from the present expansion. We are aware that this may affect the convergence of the scattering calculations.

We calculated partial-wave contributions up to $J=41/2$ numerically and used a geometric extrapolation scheme to account for even higher partial waves if necessary. The cross sections of interest were then calculated in the same way as in the standard *R*-matrix approach. We employed an updated version [43] of the flexible asymptotic *R*-matrix (FARM) package by Burke and Noble [44] to solve the problem in the asymptotic region and to obtain the transition matrix elements of interest. After transforming the latter from the present *jj*-coupling to the *jlK*-coupling scheme and also accounting for the appropriate phase convention of the reduced matrix elements, we employed the program MJK of Grum-Grzhimailo [45] to calculate the angle-differential cross sections shown below.

III. RESULTS AND DISCUSSION

In this section, we present results for angle-integrated and angle-differential cross sections. The quality of these results is assessed by comparing our predictions to a variety of experimental benchmark data and predictions from other theories.

A. Angle-integrated cross sections

Figure 1 exhibits the angle-integrated elastic and total (elastic+excitation+ionization) cross sections for electron collisions with mercury atoms in their $(6s^2)\ ^1S_0$ ground state. Overall, there is good agreement between the results from a nonrelativistic 54-state convergent close-coupling calculation [46] (CCC-54) and the current fully relativistic 36-state DBSR calculation (DBSR-36). For energies between 1 and 10 eV, the results also agree well with those from a fully relativistic polarized-orbital (RPO) method [6]. The latter is limited to elastic scattering, which however provides the dominant contribution to the total cross section in this energy regime. All theoretical predictions lie below the experimental data of Jost and Ohnemus [12], with the discrepancies ranging between a factor of about 5 at very low energies to about 30% at high energies.

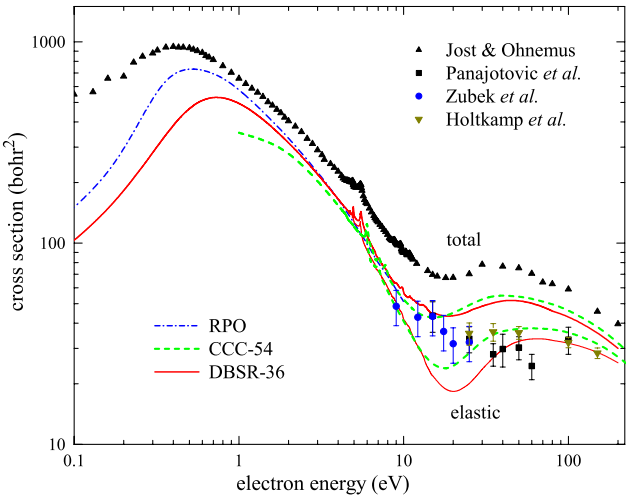

FIG. 1. (Color online) Total and elastic angle-integrated cross sections for electron scattering from mercury atoms in the $(6s^2)\ ^1S_0$ ground state. The various experimental data sets and theoretical models are described in the text.

The polarized-orbital results come closest to the experimental data for incident energies below 1 eV. We note that this energy regime is dominated by the $(6s^26p)\ ^2P^o_{1/2,3/2}$ shape resonances [6,12]. These resonances cause a maximum in the elastic cross section for incident energies between 0.4 and 0.5 eV. In our previous calculation for the similar *e*-Mg collision system [47], we demonstrated that the convergence of the close-coupling expansion for the corresponding $(3s^23p)\ ^2P^o$ resonance is extremely slow. Since the physical energy of the resonance is determined by its position *relative* to the ground state, it is actually possible to obtain a better apparent position of this resonance by reducing the quality of the ground-state description, i.e., bringing its absolute energy up relative to the resonance. It is unlikely that the reason for the discrepancy between the DBSR-36 and RPO results lies in the reduced dipole polarizability in our collision model. In fact, the RPO results were also generated with an adjusted ground-state dipole polarizability of only $23.6a_0^3$ [6]. As a final check regarding the effect of the ground-state polarizability, we performed a special calculation only for elastic scattering, in which we coupled the ground state to a number of pseudostates to assure the complete inclusion of both its dipole and quadrupole polarizabilities. The results did not change significantly from those presented in Fig. 1 for energies below 1 eV.

Although we cannot assess the reliability of the experimental results at very low energies for the reasons mentioned, it seems as if they may be somewhat too large at energies above 1 eV. This preliminary assessment is supported by the fact that the agreement between CCC-54, DBSR-36, and several sets of experimental data for the angle-integrated elastic cross section alone [14,16,17] is much better than for the total cross section. Although the minimum in the elastic cross section predicted by the theories around 20 eV is not clearly confirmed by the experimental data, it could be hidden in the size of the experimental

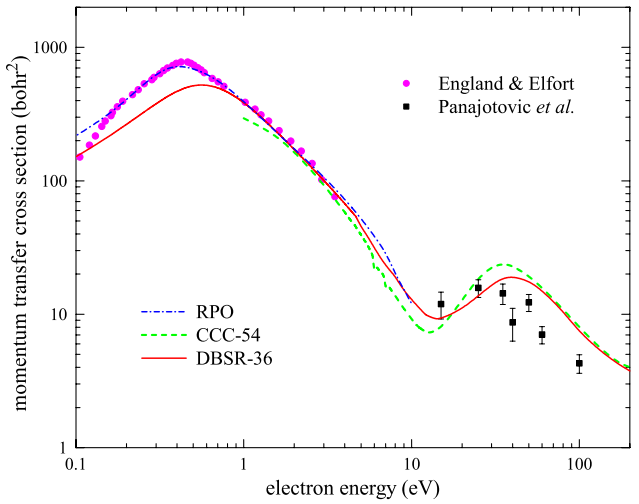

FIG. 2. (Color online) Momentum-transfer cross section for electron scattering from mercury atoms in the $(6s^2)\ ^1S_0$ ground state. The experimental data of England and Elford [13] and Panajotovic *et al.* [16] are compared to theoretical predictions from the same models as in Fig. 1.

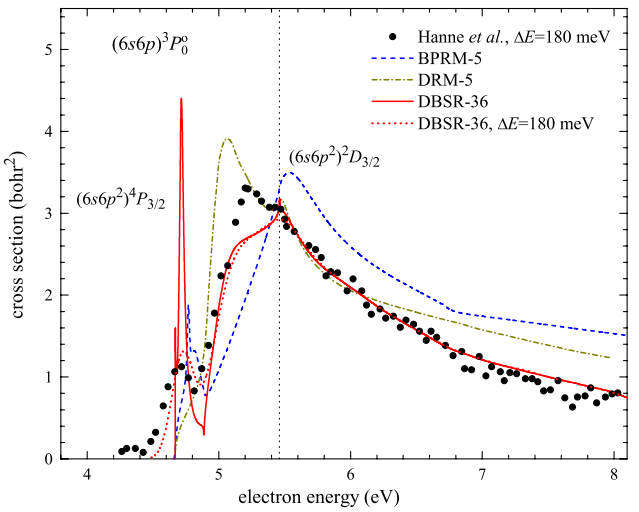

FIG. 3. (Color online) Angle-integrated cross section for electron-impact excitation of the $(6s6p)\ ^3P_0^o$ state of mercury from the $(6s^2)\ ^1S_0$ ground state. The various experimental data sets and theoretical models are described in the text.

errors bars. The existence of such a minimum is, indeed, supported by the energy dependence of the Jost and Ohnemus [12] data.

Figure 2 shows the corresponding results for the elastic momentum-transfer cross section. There is again good agreement between the CCC-54, DBSR-36, and RPO results for incident energies above 1 eV and satisfactory agreement with the experimental data of Panajotovic *et al.* [16] in the 15–100 eV regime. At the very low energies, the RPO model yields excellent agreement with the measurements of England and Elford [13], while the current DBSR-36 model produces results below experiment for incident energies of less than 1 eV. The likely reason is once again the fact that the current model predicts the position of the shape resonances too high.

Figures 3–5 compare various experimental and theoretical results for excitation of the $(6s6p)\ ^3P^o_{0,1,2}$ states for incident energies between 4.5 and 8.0 eV. In this near-threshold regime, these excitations are strongly affected by negative-ion resonances with dominant configuration $6s6p^2$, which have been classified as $^4P_{3/2}$ (4.670 eV), $^4P_{5/2}$ (4.915 eV), $^2D_{3/2}$ (5.12 eV), and $^4P_{5/2}$ (5.53 eV) [48] (and references therein). Since the fine structure in both the target states and the resonances could easily be resolved experimentally, the nonrelativistic CCC-54 model is not appropriate for this energy regime and hence no data from this calculation are available for comparison.

Comparison of the present DBSR-36 results to the experimental data of Hanne *et al.* [49] for excitation of the metastable $(6s6p)\ ^3P_0^o$ state (see Fig. 3) shows very satisfactory agreement, especially after the raw theoretical predictions have been convoluted with the experimental energy width of 180 meV (full width at half maximum, FWHM). There is a clear improvement in the agreement between experiment and the DBSR-36 theory compared to earlier five-state semirelativistic Breit-Pauli [9] (BPRM-5) and fully relativistic Dirac *R*-matrix [11] (DRM-5) calculations.

The improvement is even more prominent in the excitation function of the $(6s6p)\ ^3P_1^o$ state (see Fig. 4). Although labeled as a triplet state by the dominant spin character of its wave function, this state can decay optically to the ground state by the emission of a 254 nm uv photon. These photons, after conversion to visible light, are in fact the dominant source of light originating from mercury-based discharge lamps. Hence, understanding the details of this particular transition and its driving mechanism is crucial for modeling such lamps [23].

The current DBSR-36 results are in excellent agreement with the most recent experimental data of Erdevdi *et al.* [50], which were obtained with an energy resolution of 18 meV and hence show the threshold peak in significantly more detail than the measurements by Ottley and Kleinpoppen [51], which we show as one representative of several earlier experimental investigations of this particular excitation func-

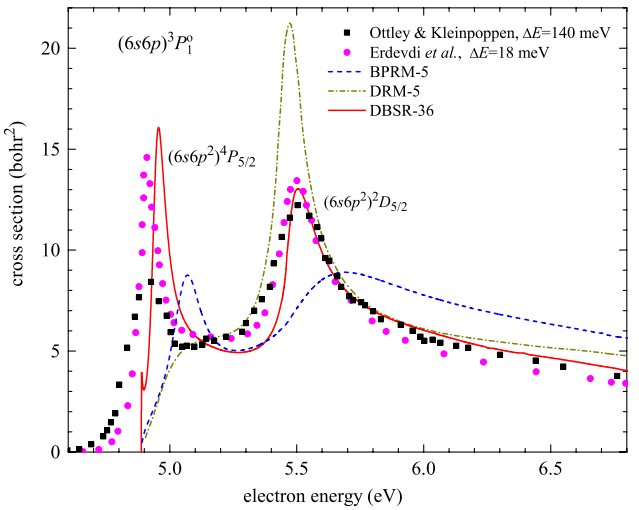

FIG. 4. (Color online) Angle-integrated cross section for electron-impact excitation of the $(6s6p)\ ^3P_1^o$ state of mercury from the $(6s^2)\ ^1S_0$ ground state. The various experimental data sets and theoretical models are described in the text.

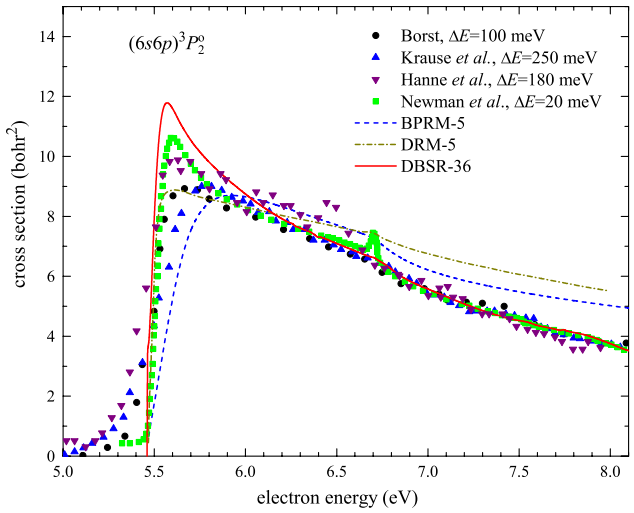

FIG. 5. (Color online) Angle-integrated cross section for electron-impact excitation of the $(6s6p)\ ^3P_2^o$ state of mercury from the $(6s^2)\ ^1S_0$ ground state. The various experimental data sets and theoretical models are described in the text.

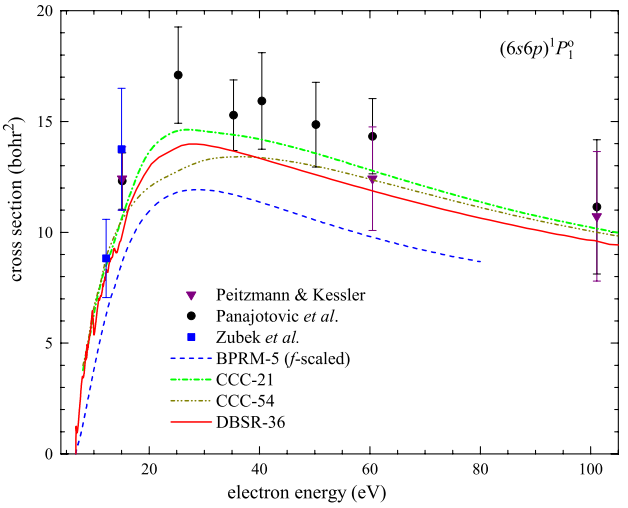

FIG. 6. (Color online) Angle-integrated cross section for electron-impact excitation of the $(6s6p)\ ^1P_1^o$ state of mercury from the $(6s^2)\ ^1S_0$ ground state. The various experimental data sets and theoretical models are described in the text.

tion. Recall that the $(6s6p^2)\ ^4P_{5/2}$ resonance in the excitation function of the $(6s6p)\ ^3P_1^o$ state is mainly responsible for the outcome of the famous Franck-Hertz experiment [52,53].

Moving on to the excitation of the metastable $(6s6p)\ ^3P_2^o$ state (see Fig. 5) shows again very satisfactory agreement of the present results with several sets of experimental data. The near-threshold maximum, caused by the $(6s6p^2)\ ^2D_{5/2}$ resonance, is best resolved in the experiment of Newman *et al.* [54], who achieved an energy resolution of 20 meV, thereby improving on earlier work by Borst [55], Krause *et al.* [56], and Hanne *et al.* [49]. The earlier BPRM-5 and DRM-5 calculations are also in good qualitative agreement with experiment, but clearly not to the extent achieved in the present work.

Table III summarizes the results for the five dominant resonances for incident energies between 4.5 and 5.5 eV, respectively. We see excellent agreement between the current predictions and the latest assignments given by Sullivan *et al.* [48]. This level of agreement gives us confidence in the correctness of our results, especially concerning this near-threshold regime.

We conclude our discussion of the angle-integrated cross sections with results for the $(6s6p)\ ^1P_1^o$ state shown in Fig. 6. Excitation of this state results in 185 nm vuv radiation. The present DBSR-36 results are in good agreement with predictions from nonrelativistic 21-state and 54-state CCC calculations [46], as well as a variety of experimental data [15,16,18]. This shows that neither relativistic effects nor channel coupling is particularly important in the theoretical description of this excitation process.

Also shown in Fig. 6 are BPRM-5 results [10]. However, the latter were rescaled using the ratio of the experimental and theoretical oscillator strengths as suggested by Kim [57]. Without this rescaling, the BPRM-5 model produces cross sections that are more than a factor of 2 larger than experiment due to the difficulty of obtaining accurate oscillator strengths using an essentially nonrelativistic structure approach without a model potential (as used in the CCC calculations) to simulate the important core-valence correlation effects. We emphasize once again that the present DBSR-36 approach accounts for these correlations in a fully *ab initio* manner.

TABLE III. Positions and widths of the $6s6p^2$ negative-ion resonances. Experimental data are taken from Sullivan *et al.* [48].

Resonance	Energy (eV)	Width (meV)	Expt.	
$(6s6p^2)\ ^4P_{1/2}$	4.614	0.04	4.550	0.46
$(6s6p^2)\ ^4P_{3/2}$	4.712	36	4.670	14.7
$(6s6p^2)\ ^4P_{5/2}$	4.938	65	4.915	60
$(6s6p^2)\ ^2D_{3/2}$	4.904	300	5.12	290
$(6s6p^2)\ ^2D_{5/2}$	5.483	148	5.53	280

B. Angle-differential cross sections

We now proceed to a comparison of angle-differential cross sections (DCS). Figure 7 exhibits the DCS for elastic electron scattering from Hg atoms at energies of 9, 15, 25, and 35 eV, respectively. A variety of experimental results [14,16,18] are compared to theoretical predictions from a relativistic distorted-wave (RDW) method [4], two nonrelativistic CCC [46] calculations, and the present DBSR-36 approach. The excellent agreement between all theories and experiments for the two highest energies of 25 and 30 eV, respectively, suggests once again that channel coupling and relativistic effects are not particularly important for these cases. At these energies, it has essentially become a potential-scattering problem, with the accuracy of the scattering potential being the decisive element that determines success or failure of a theoretical approach.

For the two lower energies of 9 and 15 eV, on the other hand, the differences between the various theoretical predic-

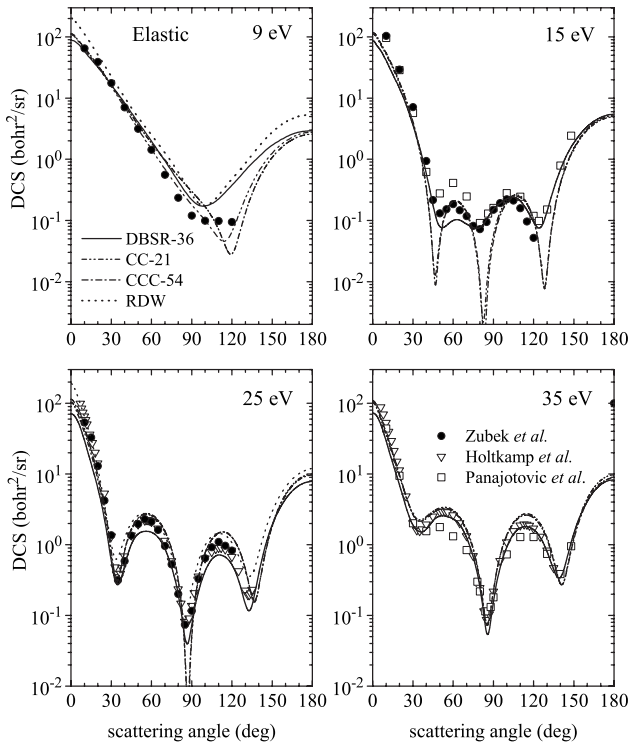

FIG. 7. Angle-differential cross section for elastic electron scattering from Hg atoms in their ground state $(6s^2)\ ^1S_0$ for energies of 9, 15, 25, and 35 eV. The various experimental data sets and theoretical models are described in the text.

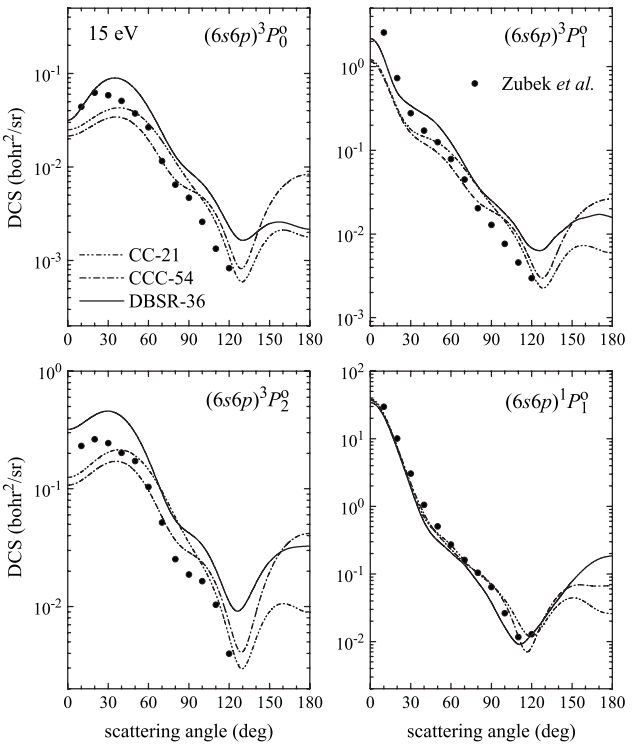

FIG. 8. Angle-differential cross section for electron-impact excitation of Hg atoms in their ground state $(6s^2)\ ^1S_0$ to the four states with dominant configuration $(6s6p)$ at an incident electron energy of 15 eV. The various experimental data sets and theoretical models are described in the text.

tions are more prominent. At 9 eV, the DBSR-36 and RDW results agree very well except near the forward direction. Both theories predict a minimum in the DCS at scattering angles just above 90°, while the two sets of CCC results show a much deeper minimum between 110° and 120°. The angular dependence seen in the experimental data of Zubek *et al.* [17] is essentially flat beyond 90° and thus no theory is favored by these data.

Finally, the present DBSR-36 results for 15 eV are in significantly better agreement with the available experimental data [16,18] than the CCC calculations [46]. Both calculations predict three minima of the DCS, in agreement with the experimental findings, but the CCC approach produces them significantly lower than DBSR-36 and also much lower than what is seen experimentally. It seems unlikely that the finite experimental angular resolution is responsible for the shallowness of the experimental minima. The only apparent problem with the DBSR-36 results at 15 eV is the local maximum around 60°, which is significantly higher in both sets of experimental data.

Figure 8 shows the angle-differential cross section for electron-impact excitation of the $(6s6p)\ ^3P_{0,1,2}$ and $(6s6p)\ ^1P_1^o$ states for at an incident electron energy of 15 eV. We see good qualitative agreement between our DBSR-36 results and the experimental data of Zubek *et al.* [18] and also the nonrelativistic CCC calculations with either 21 or 54 coupled states. Nevertheless, for the two metastable states, $^3P_0^o$ and $^3P_2^o$, our results lie significantly above both experiment and the CCC calculations. This is almost certainly due to the fact that channel coupling to the ionization continuum is very important for these transitions at this energy of about one and a half times the ionization potential. While we predict the angular dependence in agreement with experiment, the absolute values obtained by the present model are most likely too large. For this case, the inclusion of the continuum makes the CCC predictions preferable.

The situation is much better for the two excited states with total electronic angular momentum $J=1$. Except for the near-forward direction, our results still show a tendency of being larger than the experimental data and the CCC results for the $^3P_1^o$ state, while the agreement is very good for the $^1P_1^o$ state. These findings agree with the general expectation that optically allowed or strong intercombination transitions are much less affected by channel coupling than strictly spin-forbidden transitions. In these cases, having an accurate structure description, particularly concerning the oscillator strengths, is the most important criterion.

Our last example is the DCS for excitation of the two $J=1$ states at an incident energy of 60 eV. As seen from Fig. 9, the agreement between two sets of experimental data by Peitzmann and Kessler [15] and Panajotovic *et al.* [16], respectively, and theory is excellent for the $^1P_1^o$ state. The nonrelativistic CCC and fully relativistic DBSR results also agree very well with each other for the $^3P_1^o$ state, where the experimental data [16] are systematically larger than the theoretical predictions for all scattering angles above 30°. For such relatively high energy, one would expect the singlet part of the target wave function to be the dominant contributor to the excitation process. In the lowest-order approximation,

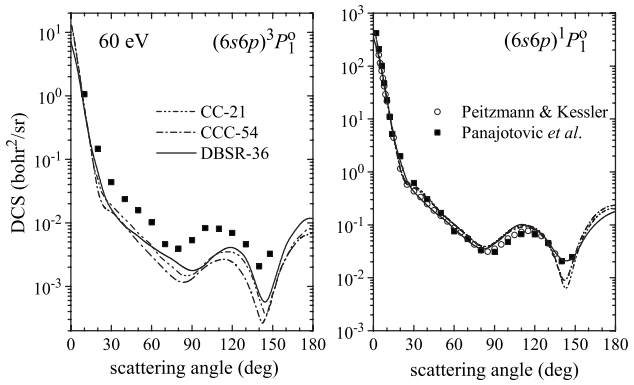

FIG. 9. Angle-differential cross section for electron-impact excitation of Hg atoms in their ground state $(6s^2)\ ^1S_0$ to the $(6s6p)\ ^{3,1}P_1^o$ states at an incident electron energy of 60 eV. The various experimental data sets and theoretical models are described in the text.

this should result in similar relative angular distributions and the absolute numbers related by the ratio of the oscillator strengths for the two transitions. The experimental ratio (see Table II) is about 50% larger than our theoretical value and that factor is approximately reflected in the results.

IV. SUMMARY AND CONCLUSIONS

In this paper, we presented results for angle-integrated and angle-differential cross sections for elastic and inelastic electron scattering from mercury atoms in their ground state $(6s^2)\ ^1S_0$. Using a fully relativistic *B*-spline *R*-matrix method with nonorthogonal orbitals and an *ab initio* account of the important core-valence correlation through coupling to states with a hole in the otherwise filled $5d$ subshell, our 36-state model obtained a significant improvement in the description of the near-threshold resonances compared to previous Breit-Pauli and Dirac close-coupling approaches. Away from threshold, our results are generally in satisfactory agreement with experiment and predictions from other state-of-the-art calculations. In some cases, such as elastic scattering at energies below 1 eV and excitation of the metastable $(6s6p)\ ^3P_0^o$ and $(6s6p)\ ^3P_2^o$ states, the accuracy of our calculation may have suffered from a slow convergence of the close-coupling expansion. As a result, the positions of some features, such as the $(6s^26p)\ ^2P_{1/2,3/2}^o$ shape resonances, are predicted somewhat too high relative to their parent state.

Work to remedy these problems is currently in progress. The basic recipe is well known from the CCC and RMPS [26,27] approaches, namely, the inclusion of a sufficient number of discrete pseudostates to represent the effect of the target continuum. In practice, however, this requires extensive further developments of our computer code, including its parallelization and thus adaption to massively parallel supercomputers. It is certainly possible, as shown recently for one-electron targets by Badnell [29]. However, we expect a major jump in complexity between Dirac-based RMPS or CCC calculations for (quasi-)one-electron systems and cases such as the one considered here, where unfilled inner shells such as $5d^9$ complicate the situation tremendously.

In the near future, we plan to further test the current model by applying it to the calculation of the spin-polarization function, various spin asymmetries, and spin-dependent electron-impact coherence parameters. As a first step, we joined forces with the Münster group and compared experimental and theoretical data for the angle-integrated Stokes parameters (light polarizations) for spin-polarized electron-impact excitation of the $(6s6p)\ ^{3,1}P_1^o$ states. The results obtained in that work are very encouraging [58].

ACKNOWLEDGMENTS

This work was supported by the United States National Science Foundation under Grants No. PHY-0555226 and No. PHY-0757755 and a Teragrid computer resource allocation under Grant No.TG-PHY090031.

[1] D. W. Walker, Adv. Phys. **20**, 257 (1971).
[2] R. P. McEachran and A. D. Stauffer, J. Phys. B **20**, 5517 (1987).
[3] J. E. Sienkiewicz, J. Phys. B **23**, 1869 (1990).
[4] J. E. Sienkiewicz, J. Phys. B **30**, 1261 (1997).
[5] R. Haberland and L. Fritsche, J. Phys. B **20**, 121 (1987).
[6] R. P. McEachran and M. T. Elford, J. Phys. B **36**, 427 (2003).
[7] K. Bartschat and D. H. Madison, J. Phys. B **20**, 1609 (1987).
[8] R. Srivastava, T. Zuo, R. P. McEachran, and A. D. Stauffer, J. Phys. B **26**, 1025 (1993).
[9] N. S. Scott, P. G. Burke, and K. Bartschat, J. Phys. B **16**, L361 (1983).
[10] K. Bartschat, in *Proceedings of the 3rd International Conference on Atomic and Molecular Data*, edited by D. R. Schultz, P. S. Krstic, and F. Ownby (AIP, New York, 2002).
[11] W. P. Wijesundera, I. P. Grant, and P. H. Norrington, J. Phys. B **25**, 2143 (1992).
[12] K. Jost and B. Ohnemus, Phys. Rev. A **19**, 641 (1979).
[13] J. P. England and M. T. Elford, Aust. J. Phys. **44**, 647 (1991).
[14] G. Holtkamp, K. Jost, F. J. Peitzmann, and J. Kessler, J. Phys. B **20**, 4543 (1987).
[15] F. J. Peitzmann and J. Kessler, J. Phys. B **23**, 2629 (1990).
[16] R. Panajotovic, V. Pejcev, M. Konstantinovic, D. Filipovic, V. Bovarski, and B. Marinkovic, J. Phys. B **26**, 1005 (1993).
[17] M. Zubek, A. Danjo, and G. C. King, J. Phys. B **28**, 4117 (1995).
[18] M. Zubek, N. Gulley, A. Danjo, and G. C. King, J. Phys. B **29**, 5927 (1996).
[19] J. Kessler, *Polarized Electrons*, 2nd ed. (Springer, New York, 1981).
[20] N. Andersen, K. Bartschat, J. T. Broad, and I. V. Hertel, Phys. Rep. **279**, 251 (1997).
[21] N. Andersen and K. Bartschat, *Polarization, Alignment, and Orientation in Atomic Collisions* (Springer, New York, 2001).

[22] J. Waymouth, *Electric Discharge Lamps* (MIT, Cambridge, MA, 1971).
[23] G. Lister, in *Low Temperature Plasma Physics: Fundamental Aspects and Applications*, edited by R. Hippler, S. Pfau, M. Schmidt, and K. H. Schoenbach (Wiley, New York, 2001), p. 387.
[24] S. D. Rockwood, Phys. Rev. A **8**, 2348 (1973).
[25] D. H. Madison, I. Bray, and I. E. McCarthy, J. Phys. B **24**, 3861 (1991).
[26] I. Bray, D. V. Fursa, A. S. Kheifets, and A. T. Stelbovics, J. Phys. B **35**, R117 (2002).
[27] K. Bartschat, E. T. Hudson, M. P. Scott, P. G. Burke, and V. M. Burke, J. Phys. B **29**, 2875 (1996).
[28] D. V. Fursa and I. Bray, Phys. Rev. Lett. **100**, 113201 (2008).
[29] N. R. Badnell, J. Phys. B **41**, 175202 (2008).
[30] O. Zatsarinny and C. Froese Fischer, J. Phys. B **33**, 313 (2000).
[31] O. Zatsarinny and K. Bartschat, J. Phys. B **37**, 2173 (2004).
[32] O. Zatsarinny and K. Bartschat, Phys. Rev. A **77**, 062701 (2008).
[33] O. Zatsarinny, Comput. Phys. Commun. **174**, 273 (2006).
[34] M. Maslov, M. J. Brunger, P. J. O. Teubner, O. Zatsarinny, K. Bartschat, D. V. Fursa, I. Bray, and R. P. McEachran, Phys. Rev. A **77**, 062711 (2008).
[35] O. Zatsarinny, K. Bartschat, M. Maslov, M. J. Brunger, and P. J. O. Teubner, Phys. Rev. A **78**, 042713 (2008).
[36] C. Froese Fischer and O. Zatsarinny, Comput. Phys. Commun. (to be published).
[37] O. Zatsarinny and C. Froese Fischer, J. Phys. B **35**, 4669 (2002).
[38] P. Jönsson, X. He, C. Froese Fischer, and I. P. Grant, Comput. Phys. Commun. **177**, 597 (2007).
[39] C. E. Moore, *Atomic Energy Levels*, NSRDS-NBS 35 (U.S. GPO, Washington, D.C., 1971), Vol. 3.
[40] R. C. M. Learner and J. Morris, J. Phys. B **4**, 1236 (1971).
[41] D. Goebel and U. Hohm, J. Phys. Chem. **100**, 7710 (1996).
[42] J. Migdalek, Phys. Scr. **T100**, 47 (2002).
[43] C. J. Noble (private communication).
[44] V. M. Burke and C. J. Noble, Comput. Phys. Commun. **85**, 471 (1995).
[45] A. N. Grum-Grzhimailo, Comput. Phys. Commun. **152**, 101 (2003).
[46] D. V. Fursa, I. Bray, and G. Lister, J. Phys. B **36**, 4255 (2003).
[47] K. Bartschat, O. Zatsarinny, I. Bray, D. V. Fursa, and A. T. Stelbovics, J. Phys. B **37**, 2617 (2004).
[48] J. P. Sullivan, P. D. Burrow, D. S. Newman, K. Bartschat, J. A. Michejda, R. Panajotovic, M. Moghbelalhossein, R. P. McEachran, and S. J. Buckman, New J. Phys. **5**, 159 (2003).
[49] G. F. Hanne, V. Nickich, and M. Sohn, J. Phys. B **18**, 2037 (1985).
[50] N. M. Erdevdi, O. B. Shpenik, and V. S. Vukstich, Opt. Spectrosc. **95**, 529 (2003).
[51] T. W. Ottley and H. Kleinpoppen, J. Phys. B **8**, 621 (1975).
[52] J. Franck and G. Hertz, Verh. Dtsch. Phys. Ges. **16**, 457 (1914).
[53] G. F. Hanne, Am. J. Phys. **56**, 696 (1988).
[54] D. S. Newman, M. Zubek, and G. King, J. Phys. B **18**, 985 (1985).
[55] W. L. Borst, Phys. Rev. **181**, 257 (1969).
[56] H. F. Krause, S. G. Johnson, and S. Datz, Phys. Rev. A **15**, 611 (1977).
[57] Y. K. Kim, Phys. Rev. A **64**, 032713 (2001).
[58] F. Jüttemann, G. F. Hanne, O. Zatsarinny, and K. Bartschat, Phys. Rev. A **79**, 042712 (2009).